

# First-principles identification of optically efficient erbium centers in GaAs

Khang Hoang\*

Center for Computationally Assisted Science and Technology & Department of Physics,  
North Dakota State University, Fargo, North Dakota 58108, United States

(Dated: March 10, 2026)

Gallium arsenide (GaAs) doped with erbium (Er), a material of interest for optoelectronics and quantum information, has been studied for decades. Yet the formation of Er luminescence centers in the semiconductor host and their properties are still not well understood. Here we present a systematic investigation of Er-related defects in GaAs, including defect complexes consisting of Er and native point defects or oxygen impurities, using first-principles hybrid-functional defect calculations. We find that these defects have electronic structure and energetics that are generally asymmetric with respect to n- and p-type doping and tend to favor electron trapping. On the basis of the calculated defect levels, formation energies, and nonradiative carrier capture coefficients, we identify Er-related defect centers that are efficient as trap-assisted nonradiative recombination centers for  $\text{Er}^{3+}$  excitation under host photoexcitation or via minority carrier injection. Our results provide an understanding for why a particular center with Er coupled to two oxygen atoms, often referred to as Er-2O, is most efficient and for the effects of n- and p-type doping and of the Er/O ratio on the formation of optically active Er centers and on the Er luminescence observed in experiments.

## I. INTRODUCTION

Semiconductors doped with rare-earth (RE) ions have long been of interest for optoelectronics and spintronics [1]. More recently, they have also been considered for quantum information applications, e.g., as single-photon emitters and spin-photon interfaces [2–6]. The materials exhibit features similar to those found in RE-doped complex oxide insulators that have been used in quantum computing and quantum memory experiments [7, 8]. These include sharp and stable intra- $4f$ -shell optical transitions and excellent coherence properties, resulting from the RE  $4f$ -electron core being well shielded by the outer  $5s^2$  and  $5p^6$  electron shells. Yet the advantage of using semiconductor hosts is that the materials can also be controlled electrically, as opposed to just optically.

Among the RE-doped semiconductors, GaAs doped with trivalent erbium ( $\text{Er}^{3+} 4f^{11}$ ) has been studied extensively experimentally [9–19], especially when codoped with oxygen [20–45]. The  $\text{Er}^{3+}$  ion offers luminescence peaks at the telecommunication wavelength (around  $1.54 \mu\text{m}$ ) originating from the  $^4I_{13/2} \rightarrow ^4I_{15/2}$  transition within the  $4f$  multiplet. Fujiwara and co-workers successfully fabricated light-emitting diodes based on (Er,O)-doped GaAs operating at room temperature [37–39]. They were also able to couple the most optically efficient (Er,O)-related defect center (referred to as “Er-2O”) to photonic crystal nanocavities or microdisk resonators and achieved up to about tenfold enhancement of Er luminescence via the Purcell effect [3–6]. Such a progress constitutes a major step toward realizing single-photon emitters or laser devices based on the material. As further discussed below, however, the formation of Er-related luminescence centers in GaAs and their properties are still not well understood. In general, whether an RE

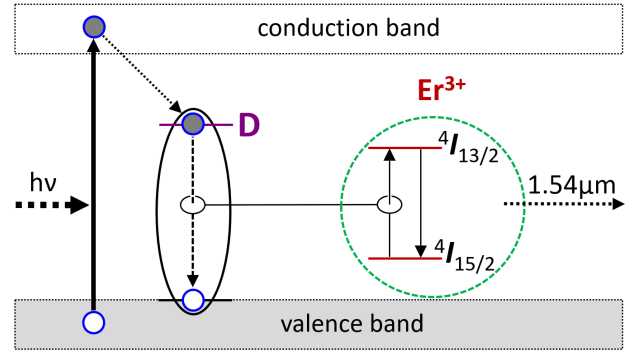


FIG. 1. Schematic illustration of indirect  $\text{Er}^{3+}$  excitation. Following band-to-band excitation of the semiconductor host, an electron is excited from the valence band to the conduction band. The excited electron is then trapped at a defect center D before recombining nonradiatively with a hole and the recombination energy is transferred into the  $\text{Er}^{3+}$   $4f$ -electron core. The same mechanism, *mutatis mutandis*, is applied to host photoexcitation involving hole trapping or when host photoexcitation is replaced with minority carrier injection.

dopant is being harnessed for traditional optoelectronic applications or for novel quantum technologies, having a detailed understanding of the interaction between the RE ion and the semiconductor host (including its native point defects, unintentional impurities, and codopants) and of the RE luminescence will assist in materials design and thus facilitate further advances in these areas.

A RE luminescence center can be optically excited by direct (resonant) intra- $4f$ -shell excitation or by indirect (nonresonant) excitation of the semiconductor host. In the former the excitation energy is directly absorbed into the  $4f$ -electron core (which is an inefficient process due to the parity-forbidden nature of the intra- $4f$ -shell optical transitions), whereas in the latter it is indirectly transferred from the host. The host excitation mecha-

\* khang.hoang@ndsu.edu

nism is expected to be mediated by defects which act as trap-assisted nonradiative recombination centers; see Fig. 1. An electron trapped at a defect center D, for instance, can recombine nonradiatively with a hole from the valence band or from some acceptor level. The recombination energy is transferred into the  $4f$ -electron core which excites an electron from one  $4f$  level (e.g.,  $^4I_{15/2}$  as seen in Fig. 1) to another ( $^4I_{13/2}$  or higher) via an Auger-type process. The excited electron in the case of  $\text{Er}^{3+}$  can then relax from  $^4I_{13/2}$  (excited state) to  $^4I_{15/2}$  (ground state) and emit a photon at  $1.54 \mu\text{m}$ . The mismatch between the nonradiative recombination energy at D and the intra- $4f$ -excitation energy is compensated by multiphonon processes. Note that, instead of excited electrons from photoexcitation of the host, electrons can be provided via minority carrier injection in a p-n junction. The defect center D, if efficient in host photoexcitation, should also be efficient when carriers are injected. Here we focus on D as an electron trap, but a similar description can be made regarding hole trapping.

For the energy transfer from the host to the RE  $4f$ -electron core to be efficient, the recombination center D needs to be in close proximity of the RE ion and the energy mismatch to be small [40, 46]. For that reason, efforts have been focused on searching for recombination centers D in which the RE ion is an integral part of D, i.e., D is a RE-related single defect or defect complex (hereafter commonly referred to as RE-related defect) [47–51]. In such a defect center, the constituent(s) other than the RE ion include localized carrier(s), native point defect(s), unintentional impurity(ies), and/or codopant(s). Strong defect–defect interaction within the RE-related defect is utilized to enhance energy transfer efficiency. Requirements for such a center are that (i) the Er-related defect induces charge-state defect transition level(s) in the band gap of the host material and (ii) the transition level(s) are suitable for high-energy recombination (e.g., in the case of  $\text{Er}^{3+}$  excitation, the nonradiative recombination energy should be at least about 0.81 eV, which is the  $^4I_{15/2} \rightarrow ^4I_{13/2}$  excitation energy), but not much higher than the intra- $4f$ -excitation energy to keep the energy mismatch small. Other features include that (iii) the carrier-capturing defect configuration is non-repulsive to minority carriers and (iv) the defect center has a relatively low formation energy. Condition (iv) is to ensure that the defect can be formed and stable, and that it can occur with a sizable concentration (although this last bit is not strictly required as only a single defect may be needed, e.g., when it is coupled to photonic crystal nanocavities for luminescence enhancement). These criteria will be made clearer in our discussions in Sec. III D.

Experimentally, Er-doped GaAs samples are often obtained by ion implantation, metal-organic chemical vapor deposition (MOCVD), or molecular beam epitaxy (MBE). Ennen et al. [9] were the first who observed fine-structured luminescence bands with sharp lines in the  $1.54\text{-}\mu\text{m}$  region in Er-implanted GaAs even at room temperature. There have been multiple experimental reports

of Er at the interstitial sites [15–19]. Kozanecki et al. [15], for example, found that as-implanted Er atoms first occupy the interstitial sites and then move to the substitutional sites after thermal annealing, and the optical activity of the Er ions (under host photoexcitation) disappears entirely after they have been located on substitutional sites. The interstitial Er defects are thus metastable. Notably, Er-doped GaAs samples often contain oxygen either as an unintentional impurity or as a codopant and, in the presence of oxygen, Er was found to be mainly (approximately) at the substitutional lattice site [24–27]. Codoping with oxygen also leads to sharper, simpler, and intense Er photoluminescence spectra [20–45].

Multiple Er luminescence centers have been observed in Er-doped GaAs (either with deliberate oxygen codoping or not) [10–12, 27–30]. Takahei and Taguchi [28], for example, observed three types of Er centers in (Er,O)-doped GaAs obtained by MOCVD: (i) Type I, first identified as an Er atom coupled to two oxygen atoms (Er-2O, with the  $C_{2v}$  symmetry) by Takahei et al. [24], shows sharp and simple photoluminescence spectra with a high intensity under host photoexcitation. (ii) Type II shows sharp and simple spectra but only under direct intra- $4f$ -shell photoexcitation and not under host photoexcitation. Several such centers were found at substantial concentrations, probably exceeding that of the Er-2O center. (iii) Type III, which was suspected to be related to Er-rich aggregates, shows complex spectra under direct intra- $4f$ -shell photoexcitation with a specific photon energy. This type of Er centers also shows luminescence under host photoexcitation but with a much lower intensity than Er-2O. Overall, Er-2O was found to dominate the luminescence spectrum under host photoexcitation [27], although it may not be the predominant defect center. Deviation from the Er:2O ratio, e.g., excessive oxygen, can lead to performance degradation [45].

It has generally been suggested that the Er-2O center acts as an electron trap [39–42], although the energy level of the trap is not entirely clear. Hogg et al. [32] deduced that the trap depth would be in the 0.82–1.22 eV region [above the valence-band maximum (VBM), if electron trapping is assumed], and Takahei et al. [40] estimated it to be at 0.42 eV [below the conduction-band minimum (CBM)]. Effects of n- or p-type doping (e.g., via S doping at the As site or Zn doping at the Ga site, respectively) has also been investigated and it was found that n-type doping greatly suppressed the formation of the Er-2O center [39] and the Er photoluminescence [34, 35].

Despite the vast experimental literature, computational investigations into Er-related defects in GaAs have been limited. Taguchi et al. [52] and Svane et al. [53] reported defect levels associated with isolated substitutional and interstitial Er defects. Coutinho et al. [54] reported results for several important (Er,O)-related defect complexes. All these previous studies, however, were based on density-functional theory (DFT) [55, 56] within the local-density approximation (LDA) [57] which are known to have limited predictive power in the study of

defects in semiconductors [50, 58, 59]. Yet the above discussion and review leave us with many questions: How do Er-2O and other Er-related defects form in GaAs and what are their atomic and electronic structure, including the trap depths induced by these defects? What make some of these defects optically efficient and why is Er-2O the best luminescence center under host photoexcitation or via minority carrier injection? There has also been a lack of understanding of the effects of n- and p-type doping and of the Er/O ratio on the formation of optically active Er centers and on the Er photoluminescence.

In this work, we report a systematic investigation of Er-related defects in GaAs, including defect complexes consisting of Er and native point defects or oxygen impurities, using state-of-the-art first-principles defect calculations [58]. Defect centers suitable for Er<sup>3+</sup> excitation, via either photoexcitation of the semiconductor host or minority carrier injection, are identified on the basis of the criteria we discussed earlier, and first-principles calculations of nonradiative carrier capture coefficients [60] are then carried out to assess their efficiency as trap-assisted recombination centers. With regard to the excitation mechanism illustrated in Fig. 1 and discussed above, we thus focus primarily on carrier capture at a defect center D and address neither the energy transfer process nor the intra-4*f*-shell transitions directly.

## II. METHODOLOGY

First-principles total-energy electronic structure calculations are based on DFT with the Heyd-Scuseria-Ernzerhof (HSE) functional [61], the projector augmented wave (PAW) method [62], and a plane-wave basis set, as implemented in VASP [63]. We use the standard PAW potentials in the VASP database which treat Ga 4*s*<sup>2</sup>4*p*<sup>1</sup>, As 4*s*<sup>2</sup>4*p*<sup>3</sup>, Er 5*s*<sup>2</sup>5*p*<sup>6</sup>4*f*<sup>12</sup>6*s*<sup>2</sup>, and O 2*s*<sup>2</sup>2*p*<sup>4</sup> explicitly as valence electrons and the rest as core electrons. The Hartree-Fock mixing parameter is set to 0.28 and the screening length to the default value of 10 Å; the plane-wave basis-set cutoff is set to 400 eV; and spin polarization is included. Defects in zincblende GaAs are simulated using 3×3×3 (216-atom) cubic supercells. Integrations over the Brillouin zone are carried out using the  $\Gamma$  point. All structural relaxations are performed with HSE and the force threshold is chosen to be 0.01 eV/Å. More computational details can be found in Ref. 59.

The formation energy of a defect X with charge state *q* (with respect to the host lattice) is defined as [58, 64]

$$E^f(X^q) = E_{\text{tot}}(X^q) - E_{\text{tot}}(\text{bulk}) - \sum_i n_i \mu_i \quad (1)$$

$$+ q(E_V + \mu_e) + \Delta^q,$$

where  $E_{\text{tot}}(X^q)$  and  $E_{\text{tot}}(\text{bulk})$  are the total energies of the defect-containing and bulk supercells;  $n_i$  is the number of atoms of species *i* that have been added ( $n_i > 0$ ) or removed ( $n_i < 0$ ) to form the defect;  $\mu_i$  is the atomic

chemical potential, representing the energy of the reservoir with which atoms are being exchanged.  $\mu_e$  is the electronic chemical potential, i.e., the Fermi level, representing the energy of the electron reservoir, referenced to the VBM of the host ( $E_V$ ). Finally,  $\Delta^q$  is the correction term to align the electrostatic potentials of the bulk and defect-containing supercells and to account for finite-size effects on the total energies of charged defects [65, 66].

The chemical potentials of Ga and As are referenced to the total energy per atom of bulk Ga and As and vary over a range determined by the formation enthalpy of GaAs:  $\mu_{\text{Ga}} + \mu_{\text{As}} = \Delta H(\text{GaAs}) = -0.96$  eV (per formula unit and calculated at 0 K) [59]. In the following presentation, we focus on the extreme Ga-rich and As-rich conditions which correspond to  $\mu_{\text{Ga}} = 0$  eV and  $\mu_{\text{As}} = 0$  eV, respectively. The chemical potential of oxygen ( $\mu_{\text{O}}$ ) is assumed to be limited by the formation of  $\beta$ -Ga<sub>2</sub>O<sub>3</sub> ( $\Delta H = -10.15$  eV) [59], and of erbium ( $\mu_{\text{Er}}$ ) by the formation of ErAs ( $\Delta H = -3.58$  eV at 0 K, compared to  $-3.28 \pm 0.14$  eV measured at 405–445° C [67]). ErAs sometimes occurs as an aggregate in Er-doped GaAs [18].

The thermodynamic transition level between charge states  $q_1$  and  $q_2$  of a defect,  $\epsilon(q_1/q_2)$ , defined as [58]

$$\epsilon(q_1/q_2) = \frac{E^f(X^{q_1}; \mu_e = 0) - E^f(X^{q_2}; \mu_e = 0)}{q_2 - q_1}, \quad (2)$$

where  $E^f(X^q; \mu_e = 0)$  is the formation energy of the defect X in charge state *q* when the Fermi level is at the VBM ( $\mu_e = 0$ ). This  $\epsilon(q_1/q_2)$  level [also referred to as the ( $q_1/q_2$ ) level], corresponding to a *defect level*, would be observed in, e.g., deep-level transient spectroscopy (DLTS) experiments where the defect in the final charge state  $q_2$  fully relaxes to its equilibrium configuration after the transition. It is evident from Eq. (2) that  $\epsilon(q_1/q_2)$  is independent of the atomic chemical potentials.

We employ the NONRAD code [68] to calculate configuration coordinate diagrams for optical transitions and nonradiative carrier capture coefficients. The code implements the first-principles approach of Alkauskas et al. [60]. Effective electron and hole masses are calculated from VASP data by using the post-processing VASPKIT package [69];  $m_e = 0.089m_0$  and  $m_h = 0.345m_0$ .

## III. RESULTS AND DISCUSSION

### A. Isolated erbium defects

Figure 2 shows the calculated formation energy of isolated substitutional and interstitial Er defects in GaAs. The substitutional Er at the Ga lattice site (Er<sub>Ga</sub>) is stable only as electrically inactive Er<sub>Ga</sub><sup>0</sup> (i.e., Er<sup>3+</sup>; spin  $S = 3/2$ ), in contrast to the results reported previously in the literature which also included the + and − charge states [52, 53]. In this configuration, Er is tetrahedrally coordinated with As; the Er–As distance is 2.70–2.71 Å, which is longer than the Ga–As bond (2.45 Å) in the bulk,

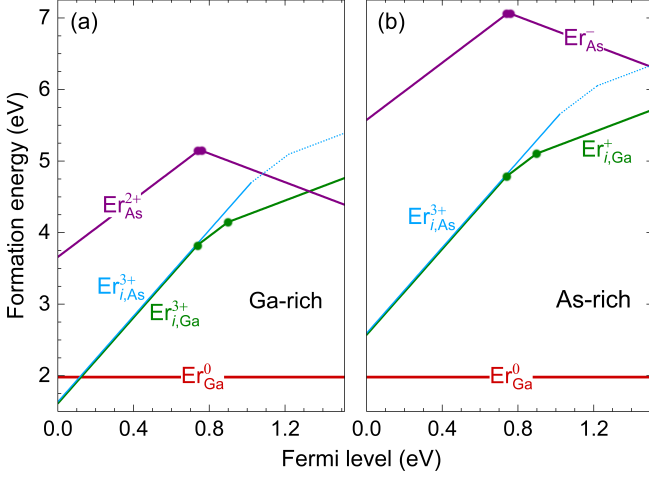


FIG. 2. Formation energies of isolated Er defects in GaAs, plotted as a function of the Fermi level from the VBM ( $E_V$ , at 0 eV) to the CBM ( $E_C$ , at 1.51 eV), under the extreme Ga-rich and As-rich conditions. For each defect, only segments corresponding to the lowest-energy charge states are shown. The slope indicates the charge state ( $q$ ): positively (negatively) charged defects have positive (negative) slopes. Large solid dots connecting two segments mark the *defect levels*. The 2+ and + charge states of  $\text{Er}_{i,\text{As}}$  are unstable.

as  $\text{Er}^{3+}$  has a larger ionic radius compared to  $\text{Ga}^{3+}$  [70]; see Fig. S1 in Appendix A. In the substitutional Er at the As site ( $\text{Er}_{\text{As}}$ ), Er is significantly off-center and becomes coordinated with three Ga and three As atoms; see Fig. S1 for the local structure of  $\text{Er}_{\text{As}}^{2+}$ . In  $\text{Er}_{i,\text{Ga}}$ , the interstitial Er atom is tetrahedrally coordinated with Ga atoms and octahedrally coordinated with As atoms (hereafter referred to as the interstitial site  $T_{\text{Ga}}$ ), whereas in  $\text{Er}_{i,\text{As}}$ , it is tetrahedrally coordinated with As and octahedrally coordinated with Ga (the  $T_{\text{As}}$  site).

In all these defect configurations, Er is stable as  $\text{Er}^{3+}$ . We find that the 2+ and + charge states of  $\text{Er}_{i,\text{As}}$  (the dotted lines in Fig. 2) and the neutral state of both  $\text{Er}_{i,\text{Ga}}$  and  $\text{Er}_{i,\text{As}}$  are electronically unstable; i.e., the  $(3+ / 2+)$  and  $(2+ / +)$  transition levels of the isolated  $\text{Er}_{i,\text{As}}$  are thus unstable. The difference between  $\text{Er}_{i,\text{Ga}}$  and  $\text{Er}_{i,\text{As}}$  is rooted in their different local lattice environments in which the local atomic (and electronic) structure of  $\text{Er}_{i,\text{As}}^{3+}$  can be regarded as being equivalent to that of  $\text{Er}_{\text{Ga}}^0$ .

Energetically,  $\text{Er}_{\text{Ga}}^0$  is most favorable among the isolated Er defects, except under the extreme Ga-rich condition where  $\text{Er}_{i,\text{Ga}}$  and  $\text{Er}_{i,\text{As}}$  have the lowest energy in a small range of Fermi-level values near the VBM, i.e., under p-type conditions; see Fig. 2(a). As one moves away from the extreme Ga-rich condition, the Er interstitials have a higher energy than  $\text{Er}_{\text{Ga}}$  even at the VBM.  $\text{Er}_{i,\text{Ga}}$  and  $\text{Er}_{i,\text{As}}$  would thus be less favorable than  $\text{Er}_{\text{Ga}}$  under realistic conditions. They are almost degenerate in energy in the 3+ charge state (As shown in Sec. III C, these two defects become more distinct when codoped with oxygen where  $\text{Er}_{i,\text{As}}\text{-O}_{\text{As}}$  has a lower formation energy

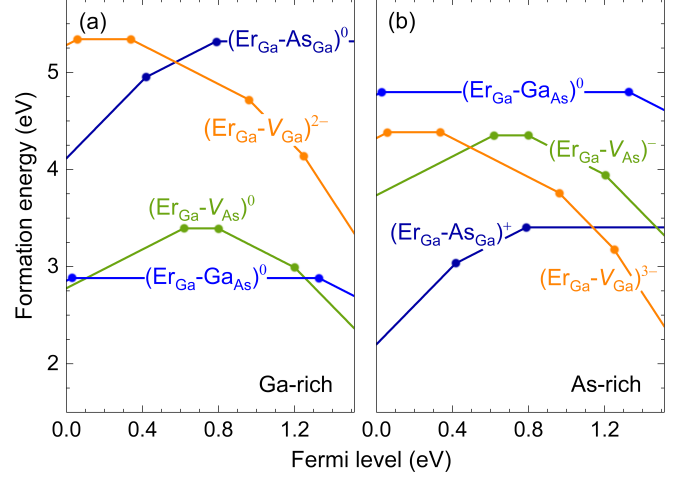


FIG. 3. Formation energies of complexes of Er and native defects under the extreme Ga-rich and As-rich conditions.

than  $\text{Er}_{i,\text{Ga}}\text{-O}_{\text{As}}$ . In other words,  $\text{Er}_{i,\text{As}}$  would be more favorable than  $\text{Er}_{i,\text{Ga}}$  when incorporated together with oxygen).  $\text{Er}_{\text{As}}$  is much higher in energy than the other isolated Er defects and thus unlikely to form.  $\text{Er}_{i,\text{Ga}}$  and  $\text{Er}_{\text{As}}$  induce defect levels in the host band gap region, see also Table S1, and are thus electrically active.

Our results are thus consistent with the metastability of Er interstitials observed in Er-implanted GaAs and the loss of the optical activity under host photoexcitation as  $\text{Er}^{3+}$  ions move from the interstitial (i.e.,  $\text{Er}_{i,\text{Ga}}$ ) to substitutional ( $\text{Er}_{\text{Ga}}$ ) sites after thermal annealing [15].

## B. Erbium-native defect complexes

Figure 3 shows the formation energy of complexes consisting of  $\text{Er}_{\text{Ga}}$  and a native point defect (i.e., the anti-site defect  $\text{Ga}_{\text{As}}$  or  $\text{As}_{\text{Ga}}$ , or the vacancy  $V_{\text{Ga}}$  or  $V_{\text{As}}$ ). A detailed investigation of the native defect constituents has already been reported in Ref. 59. Figure S1 shows the local structure of select complexes. In  $\text{Er}_{\text{Ga}}\text{-Ga}_{\text{As}}$ , both the constituents are significantly off-center with Er is three-fold coordinated with As and Ga is three-fold coordinated with Ga. In  $\text{Er}_{\text{Ga}}\text{-As}_{\text{Ga}}$ , both the constituents are four-fold coordinated and on-center. In  $\text{Er}_{\text{Ga}}\text{-V}_{\text{Ga}}$  and  $\text{Er}_{\text{Ga}}\text{-V}_{\text{As}}$ , Er is off-center and relaxes slightly toward the vacancy. We report in Table S2 the decomposition of the complex configurations into their isolated constituents.

All these Er-native defect complexes induce defect levels in the host band gap and are thus electrically active; see also Table S1. This property is largely inherited from the electrical activity of the native defect constituents [59]. The binding energy of the complexes with respect to their isolated constituents is small, however, see Table S2; and thus the complexes are unlikely to be stable and occur with a sizable concentration under thermodynamic equilibrium. As discussed in Ref. 64, in or-

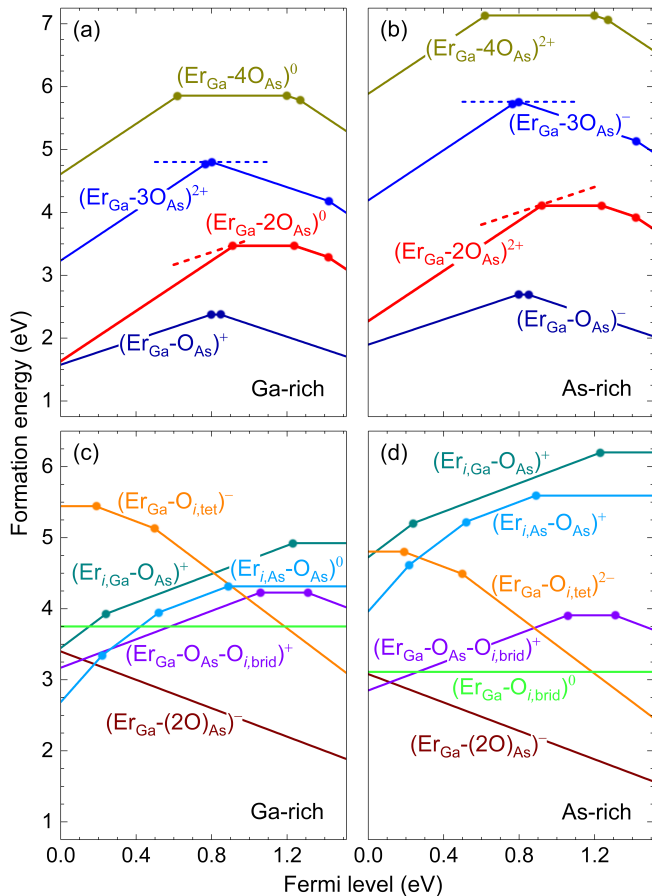


FIG. 4. Formation energies of various (Er,O)-related defect complexes in GaAs, under the extreme Ga-rich and As-rich conditions. The dashed segments represent energetically metastable (but electronically stable) charge states.

der for a defect complex to have a higher concentration than its isolated constituents, the binding energy needs to be greater than the larger of the formation energies of the isolated constituents. Although they may still form under non-equilibrium conditions where the constituents can be trapped together, we are not yet aware of any experimental report of any of these complexes.

### C. Erbium-oxygen complexes

Figure 4 shows the formation energy of various defect complexes consisting of a Er-related defect ( $\text{Er}_{\text{Ga}}$ ,  $\text{Er}_{i,\text{Ga}}$ , or  $\text{Er}_{i,\text{As}}$ ) and one or more O-related defects [specifically,  $\text{O}_{\text{As}}$ ,  $(2\text{O})_{\text{As}}$ ,  $\text{O}_{i,\text{brid}}$ , and/or  $\text{O}_{i,\text{tet}}$ ].  $\text{O}_{\text{As}}$  is the substitutional O impurity at the As lattice site;  $(2\text{O})_{\text{As}}$  is a configuration in which an As is substituted by two O atoms;  $\text{O}_{i,\text{brid}}$  is the interstitial O that bridges a Ga and an As and forms a puckered bond-center Ga–O–As structure; and  $\text{O}_{i,\text{tet}}$  is the interstitial O that is tetrahedrally coordinated with Ga. Details of the structural, electronic, and optical properties of the isolated O-related defects

can be found in Ref. 59. In the (Er,O)-related complexes, the identities of the constituent defects are largely preserved but both Er and O are significantly off-center, see Fig. S1, including those in  $\text{Er}_{\text{Ga}}-4\text{O}_{\text{As}}$ . The off-centering is mainly due to the shorter Er–O bond (and the longer Er–As bond) compared to the Ga–As bond. In  $(\text{Er}_{\text{Ga}}-2\text{O}_{\text{As}})^{2+}$ , which is the most stable configuration of  $\text{Er}_{\text{Ga}}-2\text{O}_{\text{As}}$  under p-type conditions and can be identified as the Er-2O center due to its  $C_{2v}$  symmetry, the Er–O distance (and the Er–As distance) is 2.15 Å (2.84 Å), which is comparable to that of 2.09–2.14 Å (2.76–2.81 Å) that Ofuchi et al. [26] obtained in an extended x-ray absorption fine structure (EXAFS) analysis of (Er,O)-doped GaAs samples in which the majority of Er atoms formed the Er-2O center. In the charge states from + to 2–,  $\text{Er}_{\text{Ga}}-2\text{O}_{\text{As}}$  deviates from the  $C_{2v}$  symmetry as the two Er–O bonds are no longer identical; e.g., 2.14 Å and 2.17 Å in the + state or 2.14 Å and 2.24 Å in the neutral state. The decomposition of the complex configurations into their isolated constituents is reported in Table S2.

In  $\text{Er}_{\text{Ga}}-n\text{O}_{\text{As}}$  ( $n = 1-4$ ), the defects all introduce energy levels in the host band gap, see Table S1. The defect levels induced by  $\text{Er}_{\text{Ga}}-\text{O}_{\text{As}}$  resemble those of the isolated  $\text{O}_{\text{As}}$  [59], whereas those by the other  $\text{Er}_{\text{Ga}}-n\text{O}_{\text{As}}$  complexes in the series are significantly different due to the  $\text{O}_{\text{As}}-\text{O}_{\text{As}}$  interaction. Among the other (Er,O)-related complexes,  $\text{Er}_{\text{Ga}}-\text{O}_{i,\text{brid}}$  is stable only as  $(\text{Er}_{\text{Ga}}-\text{O}_{i,\text{brid}})^0$ , which inherits the electrical inactivity of both the isolated  $\text{Er}_{\text{Ga}}$  and  $\text{O}_{i,\text{brid}}$  [59].  $\text{Er}_{\text{Ga}}-(2\text{O})_{\text{As}}$  is stable only in the – state, i.e., a shallow acceptor, determined solely by the isolated  $(2\text{O})_{\text{As}}$  [59]. In  $\text{Er}_{\text{Ga}}-\text{O}_{i,\text{tet}}$ ,  $\text{Er}_{\text{Ga}}-\text{O}_{\text{As}}-\text{O}_{i,\text{brid}}$ ,  $\text{Er}_{i,\text{Ga}}-\text{O}_{\text{As}}$ , and  $\text{Er}_{i,\text{As}}-\text{O}_{\text{As}}$ , the electrical activity of the complex also comes from that of the O constituent(s). Notably, the  $(2+/+)$  and  $(+/0)$  levels of  $\text{Er}_{\text{Ga}}-2\text{O}_{\text{As}}$  are at 0.93 eV and 0.90 eV above the VBM (see Table S1), respectively, which are within the 0.82–1.22 region deduced by Hogg et al. [32] and comparable to the trap depth at  $E_c - 0.42$  eV estimated by Takahei et al. [40].

Figure S2 shows  $\text{Er}_{\text{Ga}}-2\text{O}_{\text{As}}$  and the lowest-energy Er-related defects in GaAs, under either the extreme Ga-rich or As-rich condition, for easy comparison. We find that (Er,O)-related complexes can have an even lower formation energy than the isolated  $\text{Er}_{\text{Ga}}$ . This indicates that codoping with oxygen facilitates the incorporation of Er into the GaAs host. Oxygen has also been known to stabilize Er in GaAs and eliminate the formation of ErAs precipitates [45]. The binding energy of the defect complexes with respect to their isolated constituents are large, which is consistent with the known strong affinity of rare earths to oxygen; see Table S2. We also find that defect complexes such as  $\text{Er}_{\text{Ga}}-2\text{O}_{\text{As}}$  form most easily under p-type (and Ga-rich) conditions; see Figs. 4 and S2. In (Er,O)-doped GaAs,  $\text{Er}_{\text{Ga}}$  might be incorporated first as  $\text{Er}_{\text{Ga}}-\text{O}_{\text{As}}$ , and the complex can then capture an  $\text{O}_{\text{As}}$  to form  $\text{Er}_{\text{Ga}}-2\text{O}_{\text{As}}$ . Under n-type conditions,  $\text{Er}_{\text{Ga}}-\text{O}_{\text{As}}$  and  $\text{Er}_{\text{Ga}}-(2\text{O})_{\text{As}}$  are energetically most favorable under the Ga- and As-rich conditions, respectively, whereas the formation energy of  $\text{Er}_{\text{Ga}}-2\text{O}_{\text{As}}$  is much higher. Our re-

sults thus clearly explain why the formation of the Er-2O center is greatly suppressed in n-type doping [39].

The formation energy of  $\text{Er}_{i,\text{As}}\text{-O}_{\text{As}}$  is lower than that of  $\text{Er}_{i,\text{Ga}}\text{-O}_{\text{As}}$ , indicating that it is energetically more favorable to incorporate Er into GaAs at the interstitial site  $T_{\text{As}}$  than at the  $T_{\text{Ga}}$  site when codoped with oxygen. The 2+ and + charge states of  $\text{Er}_{i,\text{As}}$ , unstable when  $\text{Er}_{i,\text{As}}$  is in isolation, become stable in the  $\text{Er}_{i,\text{As}}\text{-O}_{\text{As}}$  complex due to the distorted lattice environment created by the presence of  $\text{O}_{\text{As}}$ . Still,  $\text{Er}_{i,\text{Ga}}\text{-O}_{\text{As}}$  and  $\text{Er}_{i,\text{As}}\text{-O}_{\text{As}}$  are much higher in energy than, e.g.,  $\text{Er}_{\text{Ga}}$ ,  $\text{Er}_{\text{Ga}}\text{-O}_{\text{As}}$ ,  $\text{Er}_{\text{Ga}}\text{-2O}_{\text{As}}$ , and  $\text{Er}_{\text{Ga}}\text{-(2O)}_{\text{As}}$ , which can explain why Er is mostly at the near-substitutional sites in (Er,O)-doped GaAs samples [24–27]. Note that  $\text{Er}_{\text{Ga}}\text{-4O}_{\text{As}}$  is also very high in energy and unlikely to occur with a sizable concentration under thermodynamic equilibrium; see Fig. 4.

For comparison, Coutinho et al. [54] reported results for  $\text{Er}_{\text{Ga}}\text{O}_{\text{As}}$  [which is  $\text{Er}_{\text{Ga}}\text{-O}_{\text{As}}$  in our notation],  $\text{Er}_{\text{Ga}}\text{O}_i$  [ $\text{Er}_{\text{Ga}}\text{-O}_{i,\text{brid}}$ ],  $\text{Er}_{\text{Ga}}(\text{O}_{\text{As}})_2$  [ $\text{Er}_{\text{Ga}}\text{-2O}_{\text{As}}$ ],  $\text{Er}_{\text{Ga}}\text{O}_{\text{As}}\text{O}_i(\text{A})$  [ $\text{Er}_{\text{Ga}}\text{-(2O)}_{\text{As}}$ ], and  $\text{Er}_{\text{Ga}}\text{O}_{\text{As}}\text{O}_i(\text{B})$  [ $\text{Er}_{\text{Ga}}\text{-O}_{\text{As}}\text{-O}_{i,\text{brid}}$ ]. Among these (Er,O)-related defect complexes, only the results for  $\text{Er}_{\text{Ga}}\text{O}_{\text{As}}$  with the reported (+/0) level at  $E_v + 0.68$  eV and the (0/−) level at  $E_c - 0.74$  eV and  $\text{Er}_{\text{Ga}}\text{O}_{\text{As}}\text{O}_i(\text{B})$  with the (+/0) level at  $E_v + 0.87$  eV and the (0/−) level at  $E_c - 0.17$  eV [54] are in qualitative agreement with our results for  $\text{Er}_{\text{Ga}}\text{-O}_{\text{As}}$  and  $\text{Er}_{\text{Ga}}\text{-O}_{i,\text{brid}}$ . The authors found that  $\text{Er}_{\text{Ga}}\text{O}_i$  induces the (+/0) level at  $E_v + 0.06$  eV and  $\text{Er}_{\text{Ga}}\text{O}_{\text{As}}\text{O}_i(\text{A})$  induces the (0/−) level at  $E_c - 1.02$  eV, which is in contrast to our results which show that  $\text{Er}_{\text{Ga}}\text{-O}_{i,\text{brid}}$  and  $\text{Er}_{\text{Ga}}\text{-(2O)}_{\text{As}}$  do not induce any defect levels in the host band gap. Notably, we find  $\text{Er}_{\text{Ga}}\text{-2O}_{\text{As}}$  induces more defect levels than just the (+/0) and (0/−) levels for  $\text{Er}_{\text{Ga}}(\text{O}_{\text{As}})_2$  reported in Ref. 54; see Fig. 4. The discrepancies can be ascribed primarily to the shortcomings of DFT-LDA [50, 58, 59].

#### D. Trap-assisted recombination centers

Our results thus far show that there are many possible Er-related defects in GaAs. The electronic structure and energetics of the defects are generally asymmetric with respect to n- and p-type doping; many have a lower formation energy under p-type conditions and defect levels that tend to favor electron trapping (i.e., with carrier-capturing configurations that are non-repulsive to electrons). Exceptions are  $\text{Er}_{\text{Ga}}\text{-V}_{\text{Ga}}$  and  $\text{Er}_{\text{Ga}}\text{-V}_{\text{As}}$ , but these complexes have a very low binding energy and are unlikely to be stable;  $\text{Er}_{\text{Ga}}\text{-O}_{i,\text{tet}}$ , but it is much higher in energy than the lowest-energy (Er,O)-related defects; and  $\text{Er}_{\text{Ga}}\text{-(2O)}_{\text{As}}$ , which does not have any defect level in the host band gap and is thus optically inactive under host photoexcitation. We will thus focus on defects and defect levels that are suitable for electron trapping. As the recombination rate is limited by the rate of the capture of minority carriers, such levels would be efficient as trap-assisted recombination centers in p-type GaAs.

Among the energy levels induced by the isolated Er-

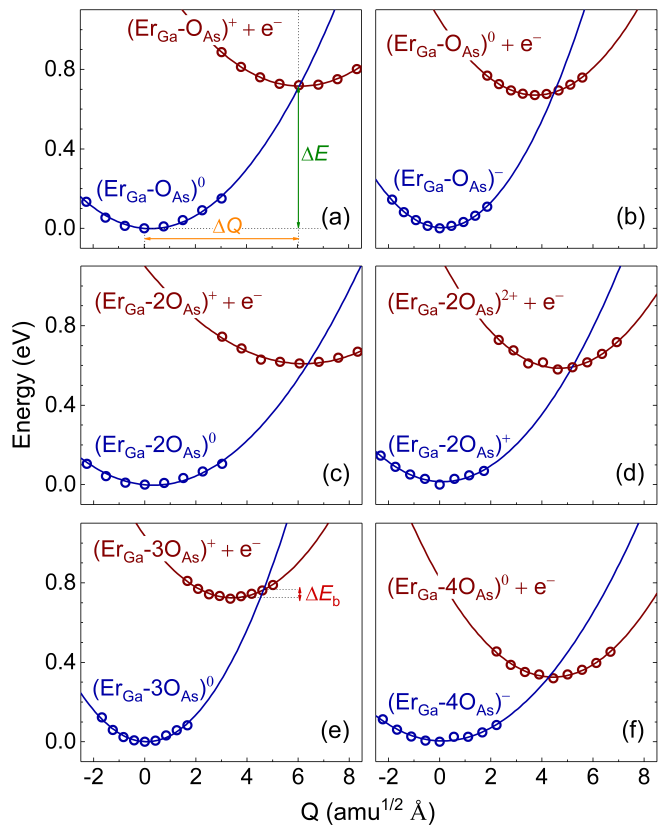


FIG. 5. Configuration coordinate diagrams for transitions involving select Er-related defect complexes in GaAs.  $\Delta E$  is the ionization energy (trap depth);  $\Delta Q$  is the mass-weighted difference between the geometries of the excited and ground states; and  $\Delta E_b$  is the (semiclassical) electron capture barrier.

related defects, only the (2 + /+) level of  $\text{Er}_{i,\text{Ga}}$ , at 0.90 eV above the VBM, is suitable as a recombination center for  $\text{Er}^{3+}$  excitation via an electron trapping mechanism. Within the Er-native defect complexes, the (0/−) level of  $\text{Er}_{\text{Ga}}\text{-Ga}_{\text{As}}$ , at 1.33 eV, would also be suitable; however, the complex is likely unstable and the mismatch between the recombination energy (1.33 eV) and the intra-4*f*-excitation energy ( $\sim 0.81$  eV) is large. Most notably, we find that the (Er,O)-related defects offer many suitable defect levels (Table S1) in which the (2 + /+) level of  $\text{Er}_{\text{Ga}}\text{-2O}_{\text{As}}$ , at 0.93 eV, emerges as an outstanding candidate for  $\text{Er}^{3+}$  excitation in p-type GaAs, based on the criteria discussed in Sec. I. The carrier-capturing configuration of this center, i.e.,  $(\text{Er}_{\text{Ga}}\text{-2O}_{\text{As}})^{2+}$ , has a low formation energy under p-type conditions, is highly attractive to the minority carriers (i.e., electrons from the conduction band), and has a small energy mismatch of  $\sim 0.1$  eV or even smaller (if one accounts for the shallow acceptor binding energy, about 30–40 meV for Be, Mg, or Zn at the Ga site or C, Si, or Ge at the As site [71]).

To quantify the ability of defect centers to capture charge carriers from the band states, we calculate their nonradiative carrier capture coefficients [60, 68]. Spe-

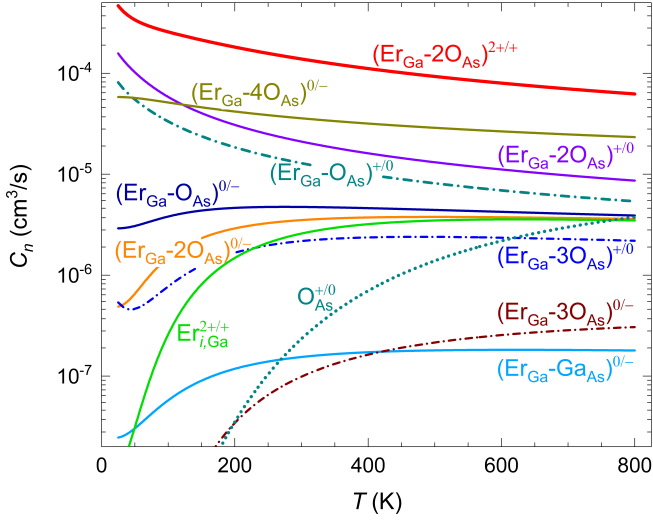


FIG. 6. Nonradiative electron capture coefficient ( $C_n$ ) at different Er-related defect centers in GaAs. Solid (dash-dotted) curves correspond to transitions with nonradiative recombination energies greater (smaller) than 0.81 eV. The result for  $O_{As}^{+/0}$  (dotted curve) is also included for comparison.

cific defects include  $Er_{i,Ga}$ ,  $Er_{Ga-Ga_{As}}$ ,  $Er_{Ga-As_{Ga}}$ ,  $Er_{Ga-nO_{As}}$  ( $n = 1-4$ ), and  $Er_{Ga-O_{As}-O_{i,brid}}$ . Some of the transition levels associated with these defects do not satisfy the condition  $\epsilon(q_1/q_2) > 0.81$  eV and some defect complexes have low binding energies but are included for comparison and to see the effect of defect association.

Figure 5 shows the configuration coordinate diagram for select transitions, obtained using the NONRAD code [68], which expresses the total energy as a function of the generalized coordinate  $Q$  which captures collective atomic displacements in an one-dimensional approximation by linear interpolation between geometries of excited and ground states [60]. Table S3 lists the parameters that appear in the nonradiative capture coefficient [60, 68]. These include the ionization energy or the trap depth ( $\Delta E$ ) which, for electron capture, is the thermodynamic transition level  $\epsilon(q_1/q_2)$  referenced to the CBM, and key parameters extracted from NONRAD calculations, including the mass-weighted difference ( $\Delta Q$ ) between the geometries of the excited (e) and ground (g) states, configurational degeneracy at the ground state ( $g_g$ ) which is the number configurations that the carrier can be captured into, energies of the effective vibrations ( $\hbar\Omega_{\{e,g\}}$ ), and electron-phonon coupling matrix elements ( $\tilde{W}_{eg}$ ).

Figure 6 shows the nonradiative electron capture coefficients ( $C_n$ ). At the  $X^{q_1/q_2}$  defect center associated with each  $C_n$  curve,  $X^{q_1}$  is the configuration into which an electron is captured. Solid  $C_n$  curves in the figure are those with  $\epsilon(q_1/q_2) > 0.81$  eV. Among the defects under consideration, we find that  $(Er_{Ga-2O_{As}})^{2+/+}$  is the most efficient center for electron capture. The highest  $C_n$  value associated with this center is resulted from having an almost zero semiclassical electron capture barrier (i.e.,

$\Delta E_b \sim 0$  eV), a large Sommerfeld parameter (due to the long-range Coulombic attraction between the electron and the doubly positively charged carrier-capturing configuration), and a relatively large electron-phonon coupling matrix element.  $(Er_{Ga-4O_{As}})^{0/-}$  also has a high capture coefficient, but it has a larger energy mismatch ( $\sim 0.3$  eV) than  $(Er_{Ga-2O_{As}})^{2+/+}$ . Notably, we find that  $Er_{i,Ga}^{2+/+}$  is as efficient as some of the (Er,O)-related centers.  $(Er_{Ga-Ga_{As}})^{0/-}$  also has a sizable electron capture coefficient value but is less efficient than most of the (Er,O)-related centers. Other centers such as  $(Er_{Ga-As_{Ga}})^{+/0}$  and  $(Er_{Ga-O_{As}-O_{i,brid}})^{+/0}$  has negligible capture coefficients (and not included in Fig. 6) mainly due to the high electron capture barrier;  $\Delta E_b \sim 1.5$  eV (in the former) or  $\infty$  (in the latter). The trend in going from  $Er_{Ga-As_{Ga}}$  to  $Er_{Ga-Ga_{As}}$  to  $Er_{Ga-O_{As}}$  follows that of the isolated  $As_{Ga}$  to  $Ga_{As}$  to  $O_{As}$  [59]. But the electron capture coefficient at  $(Er_{Ga-O_{As}})^{+}$  is about 54 times higher than that at the isolated  $O_{As}^{+}$  at room temperature, which can be ascribed in a large part to the higher semiclassical capture barrier in the latter case ( $\Delta E_b \sim 0.3$  eV [59], compared to  $\sim 0$  eV in the former). As also seen in Fig. 6, the interaction between O-related constituents in the (Er,O)-related complexes has a significant impact on nonradiative carrier capture. Note that dash-dotted  $C_n$  curves in Fig. 6 are those with  $\epsilon(q_1/q_2) < 0.81$  eV, i.e., centers with low recombination energies and thus optically inactive under host photoexcitation, but they can be excited under direct intra-4f-shell photoexcitation.

Although the capture of majority carriers is not a concern due to the high carrier concentration, we nevertheless calculate the nonradiative hole capture coefficient ( $C_p$ ) at relevant  $Er_{Ga-2O_{As}}$  and  $Er_{Ga-4O_{As}}$  configurations for comparison. Figure S3 shows that  $(Er_{Ga-2O_{As}})^{+}$  is more efficient than  $(Er_{Ga-4O_{As}})^{-}$  at capturing a hole, mainly due to the higher electron-phonon coupling matrix element in the former (more than three times higher than in the latter). Combined with the above results, this again indicates that, among the Er-related defects,  $(Er_{Ga-2O_{As}})^{2+/+}$  is overall the most efficient trap-assisted recombination center for  $Er^{3+}$  excitation, and can be identified with type-I defects discussed in Sec. I. Type-II defects are those without a defect level in the host band gap [e.g.,  $Er_{Ga}$  or  $Er_{Ga-(2O)_{As}}$ ] or those centers with an insufficient recombination energy for  $Er^{3+}$  excitation. And type-III defects may include those similar to type-I defects but with a larger energy mismatch.

Finally, regarding the effects of the Er/O ratio on the Er photoluminescence, Maltez et al. [45] found that the Er:2O ratio is optimal, whereas excessive oxygen leads to performance degradation. This appears to be consistent with our results showing that in going from  $Er_{Ga-2O_{As}}$  to  $Er_{Ga-3O_{As}}$  the defect center lose its optical activity under host photoexcitation. The reason is not just because the nonradiative capture coefficient at  $Er_{Ga-3O_{As}}$  is lower (as in Fig. 6) but, more importantly, the recombination energy at this center becomes insufficient for  $Er^{3+}$  excitation (Fig. 4). The EXAFS analysis [26] seems to suggest

the presence of optically inefficient  $\text{Er}_{\text{Ga}}\text{-3O}_{\text{As}}$  centers in (Er,O)-doped GaAs samples with a high Er concentration and a high O (low As) coordination number.

#### IV. CONCLUSIONS

We have carried out a systematic investigation of Er-related defects in GaAs using hybrid functional calculations. The defect electronic structure and energetics are found to be generally asymmetric with respect to n- and p-type doping, with many of the defects have a lower formation energy under p-type conditions and defect levels that tend to favor electron trapping. On the basis of the calculated defect levels, formation energies, and nonradiative carrier capture coefficients, we identify Er-related defect centers that are optically active under host photoexcitation or via minority carrier injection. Our results provide an understanding for why the Er-2O center is most efficient and for the effects of n- and p-type doping and of the Er/O ratio on the formation of optically active Er centers and on the Er luminescence observed in experiments. The computational approach demonstrated here can be applied to other RE-doped semiconductors

and insulators and is efficient in screening RE defects for optoelectronics and quantum information applications.

#### ACKNOWLEDGMENTS

This work used resources of the Center for Computationally Assisted Science and Technology (CCAST) at North Dakota State University, which were made possible in part by National Science Foundation Major Research Instrumentation (MRI) Award No. 2019077.

#### DATA AVAILABILITY

The data that support the findings of this study are included in this article and its appendix. Additional data are available from the author upon reasonable request.

#### Appendix A: Supplementary Material

This section includes defect local structures and formation energies and binding energies of defect complexes.

- 
- [1] K. O'Donnell and V. Dierolf, eds., *Rare Earth Doped III-Nitrides for Optoelectronic and Spintronic Applications*, Topics in Applied Physics, Vol. 124 (Springer, Dordrecht, 2010).
- [2] C. Yin, M. Rancic, G. G. de Boo, N. Stavrias, J. C. McCallum, M. J. Sellars, and S. Rogge, Optical addressing of an individual erbium ion in silicon, *Nature* **497**, 91 (2013).
- [3] M. Ogawa, J. Tatebayashi, N. Fujioka, R. Higashi, M. Fujita, S. Noda, D. Timmerman, S. Ichikawa, and Y. Fujiwara, Quantitative evaluation of enhanced Er luminescence in GaAs-based two-dimensional photonic crystal nanocavities, *Appl. Phys. Lett.* **116**, 181102 (2020).
- [4] R. Higashi, M. Ogawa, J. Tatebayashi, N. Fujioka, D. Timmerman, S. Ichikawa, and Y. Fujiwara, Enhancement of Er luminescence in microdisk resonators made of Er,O-codoped GaAs, *J. Appl. Phys.* **127**, 233101 (2020).
- [5] Z. Fang, J. Tatebayashi, R. Homi, M. Ogawa, H. Kajii, M. Kondow, K. Kitamura, B. Mitchell, S. Ichikawa, and Y. Fujiwara, Enhancement of Er luminescence from bridge-type photonic crystal nanocavities with Er, O-codoped GaAs, *Opt. Continuum* **2**, 2178 (2023).
- [6] Z. Fang, H. Kajii, M. Kondow, Y. Fujiwara, and J. Tatebayashi, Demonstration of enhanced Er luminescence in nanobeam photonic crystal nanocavities based on Er,O-codoped GaAs, *Jpn. J. Appl. Phys.* **64**, 025001 (2025).
- [7] C. Thiel, T. Böttger, and R. Cone, Rare-earth-doped materials for applications in quantum information storage and signal processing, *J. Lumin.* **131**, 353 (2011).
- [8] N. Kunkel and P. Goldner, Recent Advances in Rare Earth Doped Inorganic Crystalline Materials for Quantum Information Processing, *Z. Anorg. Allg. Chem.* **644**, 66 (2018).
- [9] H. Ennen, J. Schneider, G. Pomrenke, and A. Axmann, 1.54- $\mu\text{m}$  luminescence of erbium-implanted III-V semiconductors and silicon, *Appl. Phys. Lett.* **43**, 943 (1983).
- [10] G. S. Pomrenke, H. Ennen, and W. Haydl, Photoluminescence optimization and characteristics of the rare-earth element erbium implanted in GaAs, InP, and GaP, *J. Appl. Phys.* **59**, 601 (1986).
- [11] R. S. Smith, H. D. Müller, H. Ennen, P. Wennekers, and M. Maier, Erbium doping of molecular beam epitaxial GaAs, *Appl. Phys. Lett.* **50**, 49 (1987).
- [12] H. Ennen, J. Wagner, H. D. Müller, and R. S. Smith, Photoluminescence excitation measurements on GaAs:Er grown by molecular-beam epitaxy, *J. Appl. Phys.* **61**, 4877 (1987).
- [13] K. Thonke, H. U. Hermann, and J. Schneider, A Zeeman study of the 1.54 $\mu\text{m}$  transition in molecular beam epitaxial GaAs:Er, *J. Phys. C: Solid State Phys.* **21**, 5881 (1988).
- [14] K. Takahei, P. S. Whitney, H. Nakagome, and K. Uwai, Temperature dependence of intra-4f-shell photo- and electroluminescence spectra for erbium-doped GaAs, *J. Appl. Phys.* **65**, 1257 (1989).
- [15] A. Kozanecki, M. Chan, C. Jaynes, B. Sealy, and K. Homewood, Lattice location of erbium implanted into GaAs, *Solid State Commun.* **78**, 763 (1991).
- [16] J. Nakata, M. Taniguchi, and K. Takahei, Direct evidence of Er atoms occupying an interstitial site in metalorganic chemical vapor deposition-grown GaAs:Er, *Appl. Phys. Lett.* **61**, 2665 (1992).
- [17] J. Nakata, N. Jourdan, H. Yamaguchi, K. Takahei, Y. Yamamoto, and Y. Kido, Structural analysis of erbium sheet-doped GaAs grown by molecular-beam epitaxy, with ion channeling followed by Monte Carlo simulation,

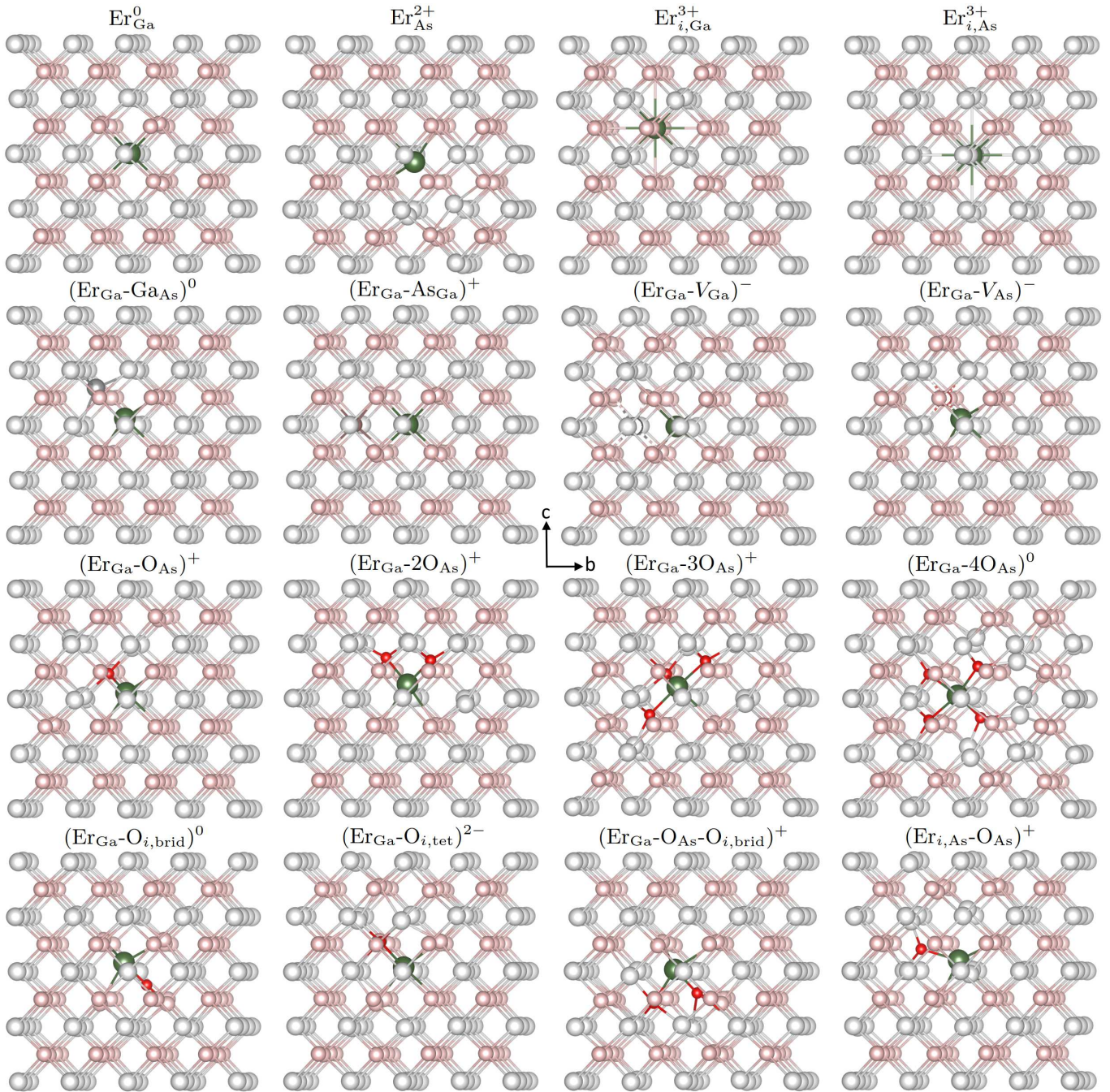


FIG. S1. Local structures of select Er-related defect configurations in GaAs. Large (gray) spheres are Ga and small (red) spheres are As where antisite Ga and As atoms are marked with slightly darker colors for easy recognition; oxygen is represented by a smaller (red) sphere. For defect complexes, see more information in Table S2.

- J. Appl. Phys. **77**, 3095 (1995).
- [18] E. Alves, M. F. da Silva, J. C. Soares, M. O. Henry, R. Gwilliam, B. J. Sealy, K. Freitag, R. Vianden, and D. Stievenard, Lattice site location of thulium and erbium implanted GaAs, Nucl. Instrum. Methods Phys. Res. B **136–138**, 421 (1998).
- [19] U. Wahl, A. Vantomme, G. Langouche, and T. ISOLDE collaboration, Lattice sites and damage annealing of Er in low-dose implanted GaAs, Nucl. Instrum. Methods Phys. Res. B **148**, 492 (1999).
- [20] H. Nakagome, K. Uwai, and K. Takahei, Extremely sharp erbium-related intra- $4f$ -shell photoluminescence of erbium-doped GaAs grown by metalorganic chemical vapor deposition, Appl. Phys. Lett. **53**, 1726 (1988).
- [21] A. Taguchi, K. Takahei, and J. Nakata, Electronic properties and their relations to optical properties in rare earth doped III-V semiconductors, in *Rare Earth Doped Semiconductors*, Mat. Res. Soc. Symp. Proc., Vol. 301

TABLE S1. Defect energy levels [ $\epsilon(q/q')$ , in eV, with respect to the VBM] induced by Er-related defects.

Defect	Defect energy levels <sup>a</sup>
Er <sub>As</sub>	(2 + /0) = 0.74, (0/-) = 0.76; (2 + /+) = 0.81, (+/0) = 0.67
Er <sub>i,Ga</sub>	(3 + /2+) = 0.74, (2 + /+) = 0.90
Er <sub>Ga</sub> -GaAs	(+/0) = 0.03, (0/-) = 1.33
Er <sub>Ga</sub> -AsGa	(2 + /+) = 0.42, (+/0) = 0.79
Er <sub>Ga</sub> -V <sub>Ga</sub>	(+/0) = 0.06, (0/-) = 0.34, (-/2-) = 0.96, (2 - /3-) = 1.25
Er <sub>Ga</sub> -V <sub>As</sub>	(+/0) = 0.62, (0/-) = 0.80, (-/2-) = 1.20
Er <sub>Ga</sub> -O <sub>i,tet</sub>	(+/0) = 0.04, (0/-) = 0.20, (-/2-) = 0.50
Er <sub>Ga</sub> -O <sub>As</sub> -O <sub>i,brid</sub>	(+/0) = 1.06, (0/-) = 1.31
Er <sub>i,Ga</sub> -O <sub>As</sub>	(2 + /+) = 0.24, (+/0) = 1.23
Er <sub>i,As</sub> -O <sub>As</sub>	(3 + /2+) = 0.22, (2 + /+) = 0.52, (+/0) = 0.89
Er <sub>Ga</sub> -O <sub>As</sub>	(+/0) = 0.80, (0/-) = 0.85
Er <sub>Ga</sub> -2O <sub>As</sub>	(2 + /0) = 0.92, (0/-) = 1.24, (-/2-) = 1.42; (2 + /+) = 0.93, (+/0) = 0.90
Er <sub>Ga</sub> -3O <sub>As</sub>	(2 + /+) = 0.77, (+/0) = 0.80, (0/-) = 0.80, (-/2-) = 1.42
Er <sub>Ga</sub> -4O <sub>As</sub>	(2 + /0) = 0.62, (0/-) = 1.20, (-/2-) = 1.27; (2 + /+) = 0.74, (+/0) = 0.51

<sup>a</sup>Electronically stable but energetically metastable defect levels, if available, are listed after the semicolon.

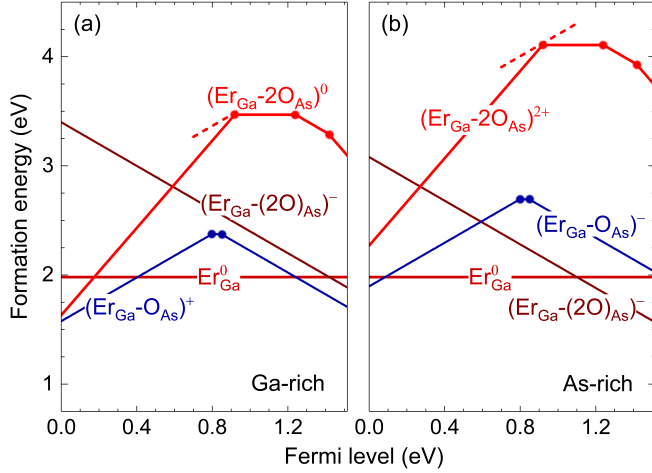


FIG. S2. Er<sub>Ga</sub>-2O<sub>As</sub> and the lowest-energy Er-related defects under either the extreme Ga-rich or As-rich condition.

(Materials Research Society, Pittsburgh, PA, 1993) pp. 139–150.

- [22] K. Takahei and A. Taguchi, Selective formation of an efficient Er-O luminescence center in GaAs by metalorganic chemical vapor deposition under an atmosphere containing oxygen, *J. Appl. Phys.* **74**, 1979 (1993).
- [23] K. Takahei and A. Taguchi, Efficient Er Luminescence Centers Formed in GaAs by Metalorganic Chemical Va-

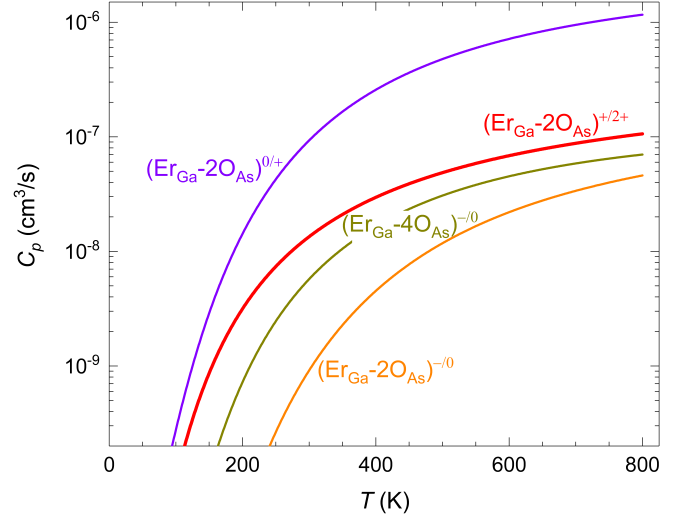


FIG. S3. Nonradiative hole capture coefficient ( $C_p$ ) at select Er-related defect centers in GaAs; see text.

por Deposition with Oxygen Codoping, *Jpn. J. Appl. Phys.* **33**, 709 (1994).

- [24] K. Takahei, A. Taguchi, Y. Horikoshi, and J. Nakata, Atomic configuration of the Er-O luminescence center in Er-doped GaAs with oxygen codoping, *J. Appl. Phys.* **76**, 4332 (1994).
- [25] J. Kaczanowski, Y. Yamamoto, Y. Kido, J. Nakata, and K. Takahei, Monte Carlo simulation of channeling spectra for compound crystals with point defects and crystalline precipitates, *Nucl. Instrum. Methods Phys. Res. Sect. B* **117**, 275 (1996).
- [26] H. Ofuchi, T. Kubo, M. Tabuchi, K. Takahei, and Y. Takeda, Local structures around Er atoms in GaAs:Er,O studied by fluorescence EXAFS and photoluminescence, *Microelectron. Eng.* **51–52**, 715 (2000).
- [27] K. Takahei, A. Taguchi, and R. A. Hogg, Atomic configurations of er centers in GaAs:Er,O and AlGaAs:Er,O studied by site-selective luminescence spectroscopy, *J. Appl. Phys.* **82**, 3997 (1997).
- [28] K. Takahei and A. Taguchi, Photoluminescence analysis of Er-doped GaAs under host photoexcitation and direct intra-4f-shell photoexcitation, *J. Appl. Phys.* **78**, 5614 (1995).
- [29] K. Takahei and A. Taguchi, Photoluminescence-excitation analysis of Er-doped GaAs grown by metalorganic vapor phase deposition, *J. Appl. Phys.* **77**, 1735 (1995).
- [30] T. Ishiyama, E. Katayama, K. Murakami, K. Takahei, and A. Taguchi, Electron spin resonance of Er-oxygen complexes in GaAs grown by metal organic chemical vapor deposition, *J. Appl. Phys.* **84**, 6782 (1998).
- [31] D. Haase, A. Dornen, K. Takahei, and A. Taguchi, Study of the Zeeman effect of Er<sup>3+</sup> in GaAs:Er,O, in *Rare Earth Doped Semiconductors II*, Mat. Res. Soc. Symp. Proc., Vol. 442 (Materials Research Society, Pittsburgh, PA, 1996) pp. 179–185.
- [32] R. A. Hogg, K. Takahei, and A. Taguchi, Photoluminescence excitation spectroscopy of GaAs:Er,O in the near-band-edge region, *J. Appl. Phys.* **79**, 8682 (1996).

TABLE S2. Stable charge states of defect complexes, their constituent defects, and binding energies ( $E_b$ ).

Complex	Constituents	$E_b$ (eV)	Complex	Constituents	$E_b$ (eV)
$(\text{Er}_{\text{Ga}}-\text{As}_{\text{Ga}})^0$	$\text{Er}_{\text{Ga}}^0 + \text{As}_{\text{Ga}}^0$	0.07	$(\text{Er}_{\text{Ga}}-\text{O}_{\text{As}})^0$	$\text{Er}_{\text{Ga}}^0 + \text{O}_{\text{As}}^0$	1.97
$(\text{Er}_{\text{Ga}}-\text{As}_{\text{Ga}})^+$	$\text{Er}_{\text{Ga}}^0 + \text{As}_{\text{Ga}}^+$	0.06	$(\text{Er}_{\text{Ga}}-\text{O}_{\text{As}})^+$	$\text{Er}_{\text{Ga}}^0 + \text{O}_{\text{As}}^+$	1.78
$(\text{Er}_{\text{Ga}}-\text{As}_{\text{Ga}})^{2+}$	$\text{Er}_{\text{As}}^0 + \text{As}_{\text{Ga}}^{2+}$	0.04	$(\text{Er}_{\text{Ga}}-\text{O}_{\text{As}})^-$	$\text{Er}_{\text{Ga}}^0 + \text{O}_{\text{As}}^-$	2.18
$(\text{Er}_{\text{Ga}}-\text{Ga}_{\text{As}})^0$	$\text{Er}_{\text{Ga}}^0 + \text{Ga}_{\text{As}}^0$	0.91	$(\text{Er}_{\text{Ga}}-2\text{O}_{\text{As}})^0$	$\text{Er}_{\text{Ga}}^0 + \text{O}_{\text{As}}^+ + \text{O}_{\text{As}}^-$	3.31
$(\text{Er}_{\text{Ga}}-\text{Ga}_{\text{As}})^+$	$\text{Er}_{\text{Ga}}^0 + \text{Ga}_{\text{As}}^+$	0.63	$(\text{Er}_{\text{Ga}}-2\text{O}_{\text{As}})^+$	$\text{Er}_{\text{Ga}}^0 + \text{O}_{\text{As}}^+ + \text{O}_{\text{As}}^0$	3.15
$(\text{Er}_{\text{Ga}}-\text{Ga}_{\text{As}})^-$	$\text{Er}_{\text{Ga}}^0 + \text{Ga}_{\text{As}}^-$	0.15	$(\text{Er}_{\text{Ga}}-2\text{O}_{\text{As}})^{2+}$	$\text{Er}_{\text{Ga}}^0 + \text{O}_{\text{As}}^+ + \text{O}_{\text{As}}^+$	3.10
$(\text{Er}_{\text{Ga}}-\text{V}_{\text{As}})^0$	$\text{Er}_{\text{Ga}}^0 + \text{V}_{\text{As}}^0$	1.52	$(\text{Er}_{\text{Ga}}-2\text{O}_{\text{As}})^-$	$\text{Er}_{\text{Ga}}^0 + \text{O}_{\text{As}}^0 + \text{O}_{\text{As}}^-$	3.05
$(\text{Er}_{\text{Ga}}-\text{V}_{\text{As}})^+$	$\text{Er}_{\text{Ga}}^0 + \text{V}_{\text{As}}^+$	1.09	$(\text{Er}_{\text{Ga}}-2\text{O}_{\text{As}})^{2-}$	$\text{Er}_{\text{Ga}}^0 + \text{O}_{\text{As}}^- + \text{O}_{\text{As}}^-$	2.70
$(\text{Er}_{\text{Ga}}-\text{V}_{\text{As}})^-$	$\text{Er}_{\text{Ga}}^0 + \text{V}_{\text{As}}^-$	1.41	$(\text{Er}_{\text{Ga}}-3\text{O}_{\text{As}})^0$	$\text{Er}_{\text{Ga}}^0 + \text{O}_{\text{As}}^+ + \text{O}_{\text{As}}^- + \text{O}_{\text{As}}^0$	4.34
$(\text{Er}_{\text{Ga}}-\text{V}_{\text{As}})^{2-}$	$\text{Er}_{\text{Ga}}^0 + \text{V}_{\text{As}}^{2-}$	1.98	$(\text{Er}_{\text{Ga}}-3\text{O}_{\text{As}})^+$	$\text{Er}_{\text{Ga}}^0 + 2\text{O}_{\text{As}}^+ + \text{O}_{\text{As}}^-$	4.15
$(\text{Er}_{\text{Ga}}-\text{V}_{\text{Ga}})^0$	$\text{Er}_{\text{Ga}}^0 + \text{V}_{\text{Ga}}^0$	0.72	$(\text{Er}_{\text{Ga}}-3\text{O}_{\text{As}})^{2+}$	$\text{Er}_{\text{Ga}}^0 + 2\text{O}_{\text{As}}^+ + \text{O}_{\text{As}}^0$	3.86
$(\text{Er}_{\text{Ga}}-\text{V}_{\text{Ga}})^+$	$\text{Er}_{\text{Ga}}^0 + \text{V}_{\text{Ga}}^+$	0.80	$(\text{Er}_{\text{Ga}}-3\text{O}_{\text{As}})^-$	$\text{Er}_{\text{Ga}}^0 + \text{O}_{\text{As}}^+ + 2\text{O}_{\text{As}}^-$	4.59
$(\text{Er}_{\text{Ga}}-\text{V}_{\text{Ga}})^-$	$\text{Er}_{\text{Ga}}^0 + \text{V}_{\text{Ga}}^-$	0.80	$(\text{Er}_{\text{Ga}}-3\text{O}_{\text{As}})^{2-}$	$\text{Er}_{\text{Ga}}^0 + \text{O}_{\text{As}}^0 + 2\text{O}_{\text{As}}^-$	4.16
$(\text{Er}_{\text{Ga}}-\text{V}_{\text{Ga}})^{2-}$	$\text{Er}_{\text{Ga}}^0 + \text{V}_{\text{Ga}}^{2-}$	0.47	$(\text{Er}_{\text{Ga}}-4\text{O}_{\text{As}})^0$	$\text{Er}_{\text{Ga}}^0 + 2\text{O}_{\text{As}}^+ + 2\text{O}_{\text{As}}^-$	5.71
$(\text{Er}_{\text{Ga}}-\text{V}_{\text{Ga}})^{3-}$	$\text{Er}_{\text{Ga}}^0 + \text{V}_{\text{Ga}}^{3-}$	0.11	$(\text{Er}_{\text{Ga}}-4\text{O}_{\text{As}})^+$	$\text{Er}_{\text{Ga}}^0 + 2\text{O}_{\text{As}}^+ + \text{O}_{\text{As}}^- + \text{O}_{\text{As}}^0$	5.16
$(\text{Er}_{\text{Ga}}-\text{O}_{i,\text{brid}})^0$	$\text{Er}_{\text{Ga}}^0 + \text{O}_{i,\text{brid}}^0$	0.78	$(\text{Er}_{\text{Ga}}-4\text{O}_{\text{As}})^{2+}$	$\text{Er}_{\text{Ga}}^0 + 3\text{O}_{\text{As}}^+ + \text{O}_{\text{As}}^0$	4.91
$(\text{Er}_{\text{Ga}}-\text{O}_{i,\text{tet}})^0$	$\text{Er}_{\text{Ga}}^0 + \text{O}_{i,\text{tet}}^0$	1.26	$(\text{Er}_{\text{Ga}}-4\text{O}_{\text{As}})^-$	$\text{Er}_{\text{Ga}}^0 + \text{O}_{\text{As}}^+ + \text{O}_{\text{As}}^0 + 2\text{O}_{\text{As}}^-$	5.50
$(\text{Er}_{\text{Ga}}-\text{O}_{i,\text{tet}})^+$	$\text{Er}_{\text{Ga}}^0 + \text{O}_{i,\text{tet}}^+$	1.26	$(\text{Er}_{\text{Ga}}-4\text{O}_{\text{As}})^{2-}$	$\text{Er}_{\text{Ga}}^0 + \text{O}_{\text{As}}^+ + 3\text{O}_{\text{As}}^-$	5.29
$(\text{Er}_{\text{Ga}}-\text{O}_{i,\text{tet}})^-$	$\text{Er}_{\text{Ga}}^0 + \text{O}_{i,\text{tet}}^-$	1.26	$(\text{Er}_{i,\text{Ga}}-\text{O}_{\text{As}})^0$	$\text{Er}_{i,\text{Ga}}^+ + \text{O}_{\text{As}}^-$	1.75
$(\text{Er}_{\text{Ga}}-\text{O}_{i,\text{tet}})^{2-}$	$\text{Er}_{\text{Ga}}^0 + \text{O}_{i,\text{tet}}^{2-}$	1.07	$(\text{Er}_{i,\text{Ga}}-\text{O}_{\text{As}})^+$	$\text{Er}_{i,\text{Ga}}^+ + \text{O}_{\text{As}}^0$	1.92
$(\text{Er}_{\text{Ga}}-(2\text{O})_{\text{As}})^-$	$\text{Er}_{\text{Ga}}^0 + (2\text{O})_{\text{As}}^-$	2.80	$(\text{Er}_{i,\text{Ga}}-\text{O}_{\text{As}})^{2+}$	$\text{Er}_{i,\text{Ga}}^+ + \text{O}_{\text{As}}^+$	1.17
$(\text{Er}_{\text{Ga}}-\text{O}_{\text{As}}-\text{O}_{i,\text{brid}})^0$	$\text{Er}_{\text{Ga}}^0 + \text{O}_{\text{As}}^0 + \text{O}_{i,\text{brid}}^0$	2.67	$(\text{Er}_{i,\text{As}}-\text{O}_{\text{As}})^0$	$\text{Er}_{i,\text{As}}^+ + \text{O}_{\text{As}}^-$	2.91
$(\text{Er}_{\text{Ga}}-\text{O}_{\text{As}}-\text{O}_{i,\text{brid}})^+$	$\text{Er}_{\text{Ga}}^0 + \text{O}_{\text{As}}^+ + \text{O}_{i,\text{brid}}^0$	2.74	$(\text{Er}_{i,\text{As}}-\text{O}_{\text{As}})^+$	$\text{Er}_{i,\text{As}}^{2+} + \text{O}_{\text{As}}^-$	2.58
$(\text{Er}_{\text{Ga}}-\text{O}_{\text{As}}-\text{O}_{i,\text{brid}})^-$	$\text{Er}_{\text{Ga}}^0 + \text{O}_{\text{As}}^- + \text{O}_{i,\text{brid}}^0$	2.42	$(\text{Er}_{i,\text{As}}-\text{O}_{\text{As}})^{2+}$	$\text{Er}_{i,\text{As}}^{3+} + \text{O}_{\text{As}}^-$	2.08
			$(\text{Er}_{i,\text{As}}-\text{O}_{\text{As}})^{3+}$	$\text{Er}_{i,\text{As}}^{3+} + \text{O}_{\text{As}}^0$	1.31

TABLE S3. Key parameters associated with the transitions considered in this work; see text.

Optical transition	$\Delta E$ (eV)	$\Delta Q$ ( $\text{amu}^{1/2}\text{\AA}$ )	$\hbar\Omega_e$ (meV)	$\hbar\Omega_g$ (meV)	$g_g$	$\tilde{W}_{\text{eg}}$ ( $\text{eV}/\text{amu}^{1/2}\text{\AA}$ )
$\text{Er}_{i,\text{Ga}}^{2+} + e^- \rightarrow \text{Er}_{i,\text{Ga}}^+$	0.62	5.47	9.26	9.69	1	$1.83 \times 10^{-2}$
$(\text{Er}_{\text{Ga}}-\text{Ga}_{\text{As}})^0 + e^- \rightarrow (\text{Er}_{\text{Ga}}-\text{Ga}_{\text{As}})^-$	0.19	2.86	11.92	10.36	1	$0.87 \times 10^{-2}$
$(\text{Er}_{\text{Ga}}-\text{As}_{\text{Ga}})^+ + e^- \rightarrow (\text{Er}_{\text{Ga}}-\text{As}_{\text{Ga}})^0$	0.73	1.71	17.55	16.93	1	$2.55 \times 10^{-2}$
$(\text{Er}_{\text{Ga}}-\text{O}_{\text{As}})^+ + e^- \rightarrow (\text{Er}_{\text{Ga}}-\text{O}_{\text{As}})^0$	0.72	6.05	12.24	13.34	1	$3.34 \times 10^{-2}$
$(\text{Er}_{\text{Ga}}-\text{O}_{\text{As}})^0 + e^- \rightarrow (\text{Er}_{\text{Ga}}-\text{O}_{\text{As}})^-$	0.67	3.72	15.03	17.25	1	$6.36 \times 10^{-2}$
$(\text{Er}_{\text{Ga}}-2\text{O}_{\text{As}})^{2+} + e^- \rightarrow (\text{Er}_{\text{Ga}}-2\text{O}_{\text{As}})^+$	0.58	4.62	14.65	13.67	2	$6.50 \times 10^{-2}$
$(\text{Er}_{\text{Ga}}-2\text{O}_{\text{As}})^+ + e^- \rightarrow (\text{Er}_{\text{Ga}}-2\text{O}_{\text{As}})^0$	0.61	6.05	10.30	11.85	1	$3.94 \times 10^{-2}$
$(\text{Er}_{\text{Ga}}-2\text{O}_{\text{As}})^0 + e^- \rightarrow (\text{Er}_{\text{Ga}}-2\text{O}_{\text{As}})^-$	0.27	4.76	13.78	13.05	1	$6.71 \times 10^{-2}$
$(\text{Er}_{\text{Ga}}-3\text{O}_{\text{As}})^+ + e^- \rightarrow (\text{Er}_{\text{Ga}}-3\text{O}_{\text{As}})^0$	0.72	3.34	14.88	17.52	2	$2.36 \times 10^{-2}$
$(\text{Er}_{\text{Ga}}-3\text{O}_{\text{As}})^0 + e^- \rightarrow (\text{Er}_{\text{Ga}}-3\text{O}_{\text{As}})^-$	0.71	9.30	11.37	10.81	1	$1.96 \times 10^{-2}$
$(\text{Er}_{\text{Ga}}-4\text{O}_{\text{As}})^0 + e^- \rightarrow (\text{Er}_{\text{Ga}}-4\text{O}_{\text{As}})^-$	0.32	4.45	14.57	12.48	2	$8.60 \times 10^{-2}$

- [33] R. A. Hogg, K. Takahei, A. Taguchi, and Y. Horikoshi, Preferential alignment of Er-2O centers in GaAs:Er,O revealed by anisotropic host-excited photoluminescence, *Appl. Phys. Lett.* **68**, 3317 (1996).
- [34] T. D. Culp, J. G. Cederberg, B. Bieg, T. F. Kuech, K. L. Bray, D. Pfeiffer, and C. H. Winter, Photoluminescence and free carrier interactions in erbium-doped GaAs, *J. Appl. Phys.* **83**, 4918 (1998).
- [35] J. G. Cederberg, T. D. Culp, B. Bieg, D. Pfeiffer, C. H. Winter, K. L. Bray, and T. F. Kuech, Incorporation of optically active erbium into GaAs using the novel precursor tris(3,5-di-tert-butylpyrazolato)bis(4-

tert-butylpyridine)erbium, *J. Appl. Phys.* **85**, 1825 (1999).

- [36] Y. Fujiwara, T. Kawamoto, T. Koide, and Y. Takeda, Luminescence properties of Er,O-codoped III-V semiconductors grown by organometallic vapor phase epitaxy, *Phys. B: Condens. Matter* **273-274**, 770 (1999).
- [37] A. Koizumi, Y. Fujiwara, A. Urakami, K. Inoue, T. Yoshikane, and Y. Takeda, Effects of active layer thickness on Er excitation cross section in GaInP/GaAs:Er,O/GaInP double heterostructure light-emitting diodes, *Phys. B: Condens. Matter* **340-342**, 309 (2003).

- [38] A. Koizumi, Y. Fujiwara, A. Urakami, K. Inoue, T. Yoshikane, and Y. Takeda, Room-temperature electroluminescence properties of Er,O-codoped GaAs injection-type light-emitting diodes grown by organometallic vapor phase epitaxy, *Appl. Phys. Lett.* **83**, 4521 (2003).
- [39] Y. Fujiwara, Room-Temperature Operation of Injection-Type 1.5  $\mu\text{m}$  Light-Emitting Diodes with Er,O-Codoped GaAs, *Mater. Trans.* **46**, 1969 (2005).
- [40] K. Takahei, R. Hogg, and A. Taguchi, Energy-transfer processes in oxygen-coped GaAs:Er, in *Rare Earth Doped Semiconductors II*, Mat. Res. Soc. Symp. Proc., Vol. 442 (Materials Research Society, Pittsburgh, PA, 1996) pp. 267–278.
- [41] K. Nakamura, S. Takemoto, Y. Terai, M. Suzuki, A. Koizumi, Y. Takeda, M. Tonouchi, and Y. Fujiwara, Direct observation of trapping of photo-excited carriers in Er,O-codoped GaAs, *Phys. B: Condens. Matter* **376–377**, 556 (2006).
- [42] M. Ishii, A. Koizumi, Y. Takeda, and Y. Fujiwara, Discrimination between energy transfer and back transfer processes for GaAs host and Er luminescent dopants using electric response analysis, *J. Appl. Phys.* **115**, 133510 (2014).
- [43] H. Katsuno, H. Ohta, O. Portugall, N. Ubrig, M. Fujisawa, F. Elmasry, S. Okubo, and Y. Fujiwara, Energy structure of Er-2O center in GaAs:Er,O studied by high magnetic field photoluminescence measurement, *J. Lumin.* **131**, 2294 (2011).
- [44] F. Elmasry, S. Okubo, H. Ohta, and Y. Fujiwara, Electron spin resonance study of Er-concentration effect in GaAs:Er,O containing charge carriers, *J. Appl. Phys.* **115**, 193904 (2014).
- [45] R. L. Maltez, E. Ribeiro, A. A. Bernussi, L. Amaral, M. Behar, P. Specht, and Z. Liliental-Weber, TEM and PL characterization of erbium and oxygen co-implanted LT-GaAs:Be, *Nucl. Instrum. Methods Phys. Res., Sect. B* **218**, 444 (2004).
- [46] T. Gregorkiewicz and J. Langer, Lasing in Rare-Earth-Doped Semiconductors: Hopes and Facts, *MRS Bulletin* **24**, 27–32 (1999).
- [47] K. Hoang, Hybrid density functional study of optically active  $\text{Er}^{3+}$  centers in GaN, *Phys. Status Solidi RRL* **9**, 722 (2015).
- [48] K. Hoang, First-principles identification of defect levels in Er-doped GaN, *Phys. Status Solidi RRL* **10**, 915 (2016).
- [49] K. Hoang, Rare-earth defects and defect-related luminescence in ZnS, *J. Appl. Phys.* **131**, 015705 (2022).
- [50] K. Hoang, Tuning the valence and concentration of europium and luminescence centers in GaN through codoping and defect association, *Phys. Rev. Materials* **5**, 034601 (2021).
- [51] K. Hoang, Rare-earth defects in GaN: A systematic investigation of the lanthanide series, *Phys. Rev. Materials* **6**, 044601 (2022).
- [52] A. Taguchi and T. Ohno, Erbium in GaAs: Coupling with native defects, *Phys. Rev. B* **56**, 9477 (1997).
- [53] A. Svane, N. E. Christensen, L. Petit, Z. Szotek, and W. M. Temmerman, Electronic structure of rare-earth impurities in GaAs and GaN, *Phys. Rev. B* **74**, 165204 (2006).
- [54] J. Coutinho, R. Jones, M. J. Shaw, P. R. Briddon, and S. Öberg, Optically active erbium–oxygen complexes in GaAs, *Appl. Phys. Lett.* **84**, 1683 (2004).
- [55] P. Hohenberg and W. Kohn, Inhomogeneous Electron Gas, *Phys. Rev.* **136**, B864 (1964).
- [56] W. Kohn and L. J. Sham, Self-Consistent Equations Including Exchange and Correlation Effects, *Phys. Rev.* **140**, A1133 (1965).
- [57] D. M. Ceperley and B. J. Alder, Ground State of the Electron Gas by a Stochastic Method, *Phys. Rev. Lett.* **45**, 566 (1980).
- [58] C. Freysoldt, B. Grabowski, T. Hickel, J. Neugebauer, G. Kresse, A. Janotti, and C. G. Van de Walle, First-principles calculations for point defects in solids, *Rev. Mod. Phys.* **86**, 253 (2014).
- [59] K. Hoang, First-principles characterization of native defects and oxygen impurities in GaAs (2025), arXiv:2506.07954 [cond-mat.mtrl-sci].
- [60] A. Alkauskas, Q. Yan, and C. G. Van de Walle, First-principles theory of nonradiative carrier capture via multiphonon emission, *Phys. Rev. B* **90**, 075202 (2014).
- [61] J. Heyd, G. E. Scuseria, and M. Ernzerhof, Hybrid functionals based on a screened Coulomb potential, *J. Chem. Phys.* **118**, 8207 (2003).
- [62] G. Kresse and D. Joubert, From ultrasoft pseudopotentials to the projector augmented-wave method, *Phys. Rev. B* **59**, 1758 (1999).
- [63] G. Kresse and J. Furthmüller, Efficient iterative schemes for ab initio total-energy calculations using a plane-wave basis set, *Phys. Rev. B* **54**, 11169 (1996).
- [64] C. G. Van de Walle and J. Neugebauer, First-principles calculations for defects and impurities: Applications to III-nitrides, *J. Appl. Phys.* **95**, 3851 (2004).
- [65] C. Freysoldt, J. Neugebauer, and C. G. Van de Walle, Fully *Ab Initio* Finite-Size Corrections for Charged-Defect Supercell Calculations, *Phys. Rev. Lett.* **102**, 016402 (2009).
- [66] C. Freysoldt, J. Neugebauer, and C. G. Van de Walle, Electrostatic interactions between charged defects in supercells, *phys. status solidi (b)* **248**, 1067 (2011).
- [67] R. Hanks and M. M. Faktor, Quantitative application of dynamic differential calorimetry. Part 2.—Heats of formation of the group 3A arsenides, *Trans. Faraday Soc.* **63**, 1130 (1967).
- [68] M. E. Turiansky, A. Alkauskas, M. Engel, G. Kresse, D. Wickramaratne, J.-X. Shen, C. E. Dreyer, and C. G. Van de Walle, Nonrad: Computing nonradiative capture coefficients from first principles, *Comput. Phys. Commun.* **267**, 108056 (2021).
- [69] V. Wang, N. Xu, J.-C. Liu, G. Tang, and W.-T. Geng, VASPKIT: A user-friendly interface facilitating high-throughput computing and analysis using VASP code, *Comput. Phys. Commun.* **267**, 108033 (2021).
- [70] R. D. Shannon, Revised effective ionic radii and systematic studies of interatomic distances in halides and chalcogenides, *Acta Crystallogr., Sect. A: Found. Crystallogr.* **32**, 751 (1976).
- [71] V. Fiorentini, Effective-mass single and double acceptor spectra in GaAs, *Phys. Rev. B* **51**, 10161 (1995).